energies

Article

A Closed-Loop Water Management Methodology for PEM Fuel Cell System Based on Impedance Information Feedback

Xinjie Xu, Kai Li *, Zhenjie Liao, Jishen Cao and Renkang Wang

School of Automation Engineering, University of Electronic Science and Technology of China, Chengdu 611731, China
* Correspondence: kaili@uestc.edu.cn

Abstract: Water management is an important issue for proton exchange membrane fuel cells (PEMFC). The research mainly focuses on the diagnosis and treatment of faults. However, faults harm PEMFC and cause its durability decay, whatever duration they last. This study designs a closed-loop water management system to control the water content in a reasonable range which can not only avoid the faults of hydration and flooding but also improve the performance and durability of PEMFC. The proposed system introduces the measurement methodology based on the phase of single-frequency impedance, which corresponds numerically well with the water content. Moreover, two preferred operating conditions, cathode air stoichiometry and stack temperature, are adopted to regulate the water content with a trade-off between the time cost and power loss. The open-loop characteristics of water content on the temperature and air stoichiometry are studied to design the corresponding control strategy. Findings suggest that air stoichiometry is suitable for large regulation requirements of water content, while the temperature is suitable to meet small demands. Finally, the proposed closed-loop water management system is validated by experiments in variable-load and constant-load with disturbance situations. The results indicate that the proposed system effectively controls the water content within a 3% deviation from the desired value.

Keywords: PEMFC; water management; impedance; phase angle; air stoichiometry; temperature

Citation: Xu, X.; Li, K.; Liao, Z.; Cao, J.; Wang, R. A Closed-Loop Water Management Methodology for PEM Fuel Cell System Based on Impedance Information Feedback. *Energies* **2022**, *15*, 7561. https://doi.org/10.3390/en15207561

Academic Editor: Ivan Tolj

Received: 17 September 2022
Accepted: 4 October 2022
Published: 13 October 2022

1. Introduction

Proton exchange membrane fuel cells (PEMFC) have received much attention in the fuel cell (FC) field because of their high-power density. Performance and durability are the key design criteria for PEMFC [1–3]. In the automotive application, where PEMFC is widely adopted, the performance and durability of PEMFC must be guaranteed. Unfortunately, the performance and durability are usually degraded by faults such as dehydration and flooding [4]. Dehydration causes a decrease in membrane conductivity, increases the internal resistance of the stack, and severely results in membrane tearing [5,6]. In contrast, the accumulation of excess liquid water causes flooding, which blocks the internal gas supply, reduces the active area of the catalyst, and eventually results in the degradation of PEMFC [7–9]. In the automotive application, PEMFC often encounters cyclic variations in load current and fluctuations in operating conditions. Both conditions can cause large fluctuations in water content, leading to dehydration and flooding [10].

Some water management approaches have been designed to deal with faults over the decades. Lebreton et al. [5] employed a self-tuning PID controller to design an active fault tolerant control strategy. Yan et al. [11] also developed an active fault tolerant control strategy with the DRT-based (distribution of relaxation times) fault diagnosis. However, they focus on handling faults when dehydration or flooding occurs. Faults harm the stack and cause its durability decay [12], whatever duration they last. To avoid dehydration and flooding, fluctuations in water content must be suppressed in time. The closed-loop water management capable of effectively controlling the water content within a reasonable range can prevent faults, ensure the stack's performance, and help improve its durability [4].

Researchers have devoted much to the study of closed-loop water management. However, there are some difficulties for a water management system to control the water content in a reasonable range. All the difficulties are related to the application scenario of the water management system. The proposed closed-loop water management system is designed for FC power systems applied to the transportation field. The water content measurement approach and control strategy are the key to the water management system. The difficulties of the water content measurement approach are the test speed and the ability to characterize the water content effectively. The difficulties of the control strategy are achieving a trade-off between time cost and power loss while ensuring that it can be widely adopted in the FC power systems.

For closed-loop water management approaches, accurate water content measurement is the basis for reasonable control. There are many approaches for water content measurement, such as electrochemical impedance spectroscopy (EIS) [13–15], pressure drop-based measurement [16], and water transport visualization techniques [17]. The water transport visualization techniques are more suited to the laboratory than automotive applications because of the equipment size and the principle. Pure pressure drop-based measurement is difficult in characterizing low water content [18]. EIS is based on the AC impedance information of PEMFC to measure water content indirectly. According to the number of test points, EIS can be divided into full-frequency spectrums [8], multiple-frequency spectrums [19], and single-frequency impedance [20]. It takes a long time to obtain the impedance at a low frequency. Therefore, the full-frequency and the multiple-frequency EIS with low-frequency points are not suitable for applications in the transportation field. Some researchers have focused on how to achieve rapid and effective measurements of EIS [20,21]. Kitamura et al. [20] utilized the high-frequency impedance at 300 Hz to characterize the water content. When the water content decreases, the high-frequency impedance rises significantly. However, the experimental results of [22] showed that the high-frequency impedance was nearly constant when PEMFC was well-humidified. The high-frequency impedance is defective in characterizing the excessive water content. Therefore, there is a requirement for the other AC impedance information, which corresponds numerically well to the water content.

In water management approaches, control strategies of water management generally adjust the operating conditions to influence the water content [5,11,23–25]. The water content can be affected by many operating conditions, such as air stoichiometry and stack temperature [26]. Santarelli et al. [26] proved the excellent ability of air stoichiometry to influence water content at high current densities. Amirinejad et al. [27] explained the effect of stack temperature on the water content and performance of PEMFC. However, there are differences in the ability of various operating conditions to regulate water content [28]. Most researchers adopted only one operation condition [19,29] to reduce the control strategy design's difficulty. However, the mismatch between regulatory requirements and operating conditions lead to a rise in time cost or power loss. The low time cost of regulation contributes to reducing the impact on stack performance caused by operating point fluctuations. The high-power loss decreases the efficiency of PEMFC [30]. In contrast, according to the ability of various operating conditions to regulate water content, matching the regulation requirements and operating conditions can make a trade-off between time cost and power loss.

Advanced control strategies are commonly designed based on the simulation models of PEMFC. Zhang et al. [23] investigated a model predictive controller to keep the cathode water content in a reasonable range. Chen et al. [24] designed an Active Disturbance Rejection Controller based on a dynamic water management model to control the humidity of the cathode. However, both approaches remain at the simulation level and are difficult to be widely used in the transportation field.

Therefore, to fill the gaps in the above studies, this paper proposes a closed-loop water management system based on the feedback value of stack impedance information, which can control the water content within the target range. To characterize the water content

and correspond numerically well with it, the system introduces the measurement method based on the phase of single-frequency impedance. Two preferred operating conditions, air stoichiometry and stack temperature, are adopted to regulate water content and achieve a trade-off between power loss and time cost. We design the control strategy with two PI controllers of both operating conditions to ensure the proposed water management system can be widely applied in the transportation field. Unlike the engineering rectification method, we obtain the open-loop transfer functions between the two operating conditions and the water content. Based on the above transfer functions, we designed PI parameters via a theoretical calculation approach to achieve accurate regulation of water content.

The rest of this paper is organized as follows. Section 2 introduces the FC system used in this study. Section 3 describes the design of the closed-loop water management system in detail. The experiments and discussions are presented in Section 4 to verify the effectiveness of the proposed water management system. The conclusions are provided in Section 5.

2. Fuel Cell System

2.1. System Structure

The overall structure of the FC system is illustrated in Figure 1, which contains the FC test system and the proposed closed-loop water management system. The FC test system contains:

- A temperature control module.
- An air stoichiometry control module.
- A stack.
- An impedance measurement module.

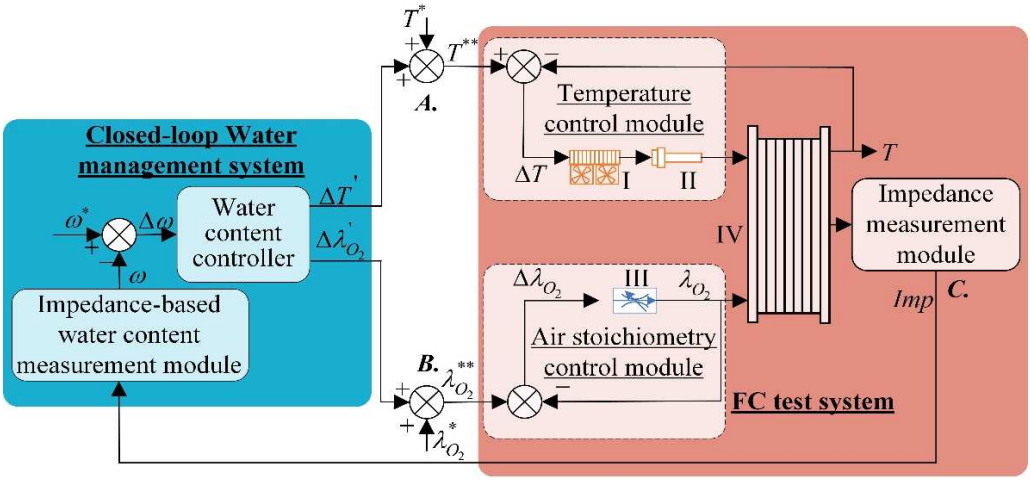

Figure 1. Overall structure of the FC system. The orange part is the FC test system, and the blue part is the closed-loop water management system. I is the radiator. II is the heater in the water tank. III is the MFC. IV is the stack. T^* and λ_{O2}^* are the set value of temperature and air stoichiometry, respectively. $\Delta T'$ and $\Delta\lambda_{O2}'$ are the corrected temperature and air stoichiometry values, respectively. T and λ_{O2} are the feedback values of temperature and air stoichiometry, respectively. T^{**} is the output of the comparator at point A. λ_{O2}^{**} is the output of the comparator at point B. ΔT is the deviation of T^{**} and T. $\Delta\lambda_{O2}$ is the deviation of λ_{O2}^{**} and λ_{O2}. *Imp* is impedance information. Ω is the feedback value of the adopted impedance information, while ω^* is its set value. $\Delta\omega$ is the deviation of ω^* and ω.

The applied stack is water-cooled with an effective reaction area of 82.56 cm^2. A mass flow controller (MFC) is equipped to regulate air stoichiometry. Because of the limited heat-producing capability of the stack used in the experiments, the temperature control system contains not only a radiator but also a heater. In Figure 1, the temperature of the stack's coolant outlet is served as T. Stack temperature can be controlled by adjusting the

fan's speed in the radiator or the heater's power according to ΔT. The sensor measured value of the MFC is the air mass flow Q. Q is converted to air stoichiometry in this study. The relationship between air stoichiometry λ_{O2} and the mass flow of supplied air Q is expressed as [31]:

$$Q = \frac{I_{st} n}{4F} \lambda_{O_2} \quad (1)$$

where I_{st} is the current, n is the number of cells, and F is the Faraday constant. Air stoichiometry is controlled by changing the opening of the regulator valve in the MFC, according to $\Delta\lambda_{O2}$. The impedance measurement module calculates the impedance *Imp* according to the stack's output. *Imp* is abundant, including the amplitude and phase angle at different frequencies. The water management system contains the impedance-based water content measurement module and water content controller. The function of the water management system is to calculate the $\Delta T'$ and $\Delta\lambda_{O2}'$ and superimpose them to the FC test system according to the *Imp*. The detailed elements of the water management system are designed in Section 3.2.2.

2.2. Impedance Measurement Module

The detailed impedance measurement module is shown in Figure 2. The programmable load applies a disturbed current $I_{measure}$ to PEMFC according to the AC demand I_{set}, which makes PEMFC generate a response voltage $V_{measure}$. Through analyzing the phase and amplitude relationship between $I_{measure}$ and $V_{measure}$, the frequency response analyzer calculates the impedance information of the corresponding frequency. The impedance information *Imp* is output to the water management system. The frequency response analyzer is the FRA32M device in PGSTAT304. The programmable load is the Chroma63205A.

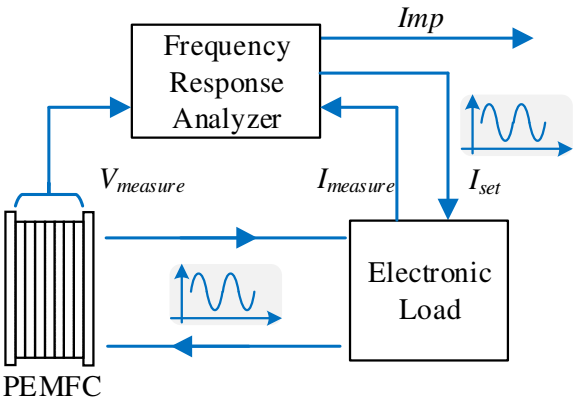

Figure 2. Detailed scheme of the impedance measurement module. *Imp* is impedance information. $V_{measure}$ is the response voltage generated by the stack. $I_{measure}$ is the disturbed current measured from the electronic load. I_{set} is the command of the current sent by frequency response analyzer to the electronic load.

3. Design of the Closed-Loop Water Management System

The water management system contains the impedance-based water content measurement module and the water content controller. The impedance-based water content measurement module is designed to adopt a piece of impedance information from *Imp* for the characterization of water content. The water content controller is designed to calculate the corrected values $\Delta T'$ and $\Delta\lambda_{O2}'$.

3.1. Design of the Impedance-Based Water Content Measurement Module

Accurate measurement of water content is the basis for adequate control in the closed-loop water management system. It is necessary to ensure that the adopted impedance information corresponds well to the water content in numerical terms. Therefore, we introduce the phase of the single-frequency impedance in the middle frequency band to

characterize the water content. Our previous work [32] verified that the phase angles of the applied stack's impedance in the 10–100 Hz band correspond well to the water content and distinguish well between different states of water content. As shown in Figure 3, the phase angle value in the 10–100 Hz band decreases when the water content decreases. In contrast, the phase angle value increases when the water content increases. The phase angle at 45 Hz has the characteristics of strong anti-interference ability and good measurement repeatability. Therefore, the phase angle at 45 Hz is adopted to characterize the water content, which is recorded as θ_{45Hz}. ω, ω^*, and $\Delta\omega$ mentioned in Figure 1 are replaced by θ_{45Hz}, θ^*_{45Hz}, and $\Delta\theta$, respectively.

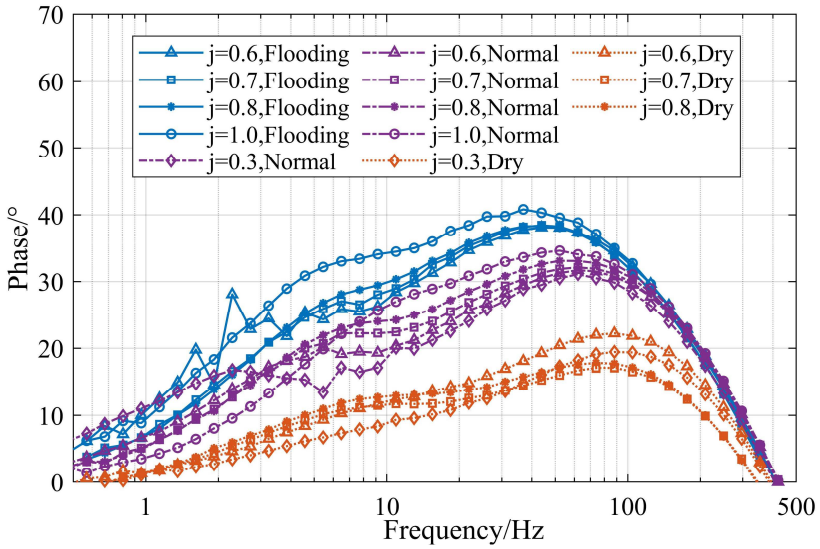

Figure 3. Phase-frequency curves at different current densities. The horizontal coordinate is the frequency. Blue, purple, and orange curves record the phase angle values in the 0.1–500 Hz band when the stack is in flooding, normal, and dehydration states, respectively. As listed in the legend, different stack states occur in different current densities.

θ^*_{45Hz} represents the water content when the regulation is completed. Therefore, θ^*_{45Hz} must correspond to normal water content. As shown in Figure 3, water content is normal when θ_{45Hz} is at [28.8°, 34.3°]. Therefore, we set a median value 31° of this interval as θ^*_{45Hz}.

3.2. Design of the Water Content Controller

3.2.1. Research on the Open-Loop Characteristics of Water Content

To design the water content controller, it is necessary to understand the dynamic characteristics of the water content. As shown in Figure 1, research on the open-loop characteristics of water content is divided into two processes. From point A to point C, the response of θ_{45Hz} to a change in T^* represents the dynamic characteristics of water content to stack temperature. From point B to point C, the response of θ_{45Hz} to a change in $\lambda_{O2}{}^*$ represents the dynamic characteristics of water content to air stoichiometry.

Table 1 lists the experimental parameters for dynamic characteristics of water content. The initial operating conditions and value of θ_{45Hz} are consistent across both sets of experiments. In each set of experiments, only one operating condition is changed. For our applied stack, the common operating range of air stoichiometry is 2.3–3.5, and the temperature range is 55–65 °C. Therefore, we set the initial T^* to 60 °C and its change to 5°C. We set the initial λ_{O2} to 2.9 and its change to 0.6.

Table 1. Experimental parameters for dynamic characteristics of water content.

Parameters	Value
Current density ($A \cdot cm^{-2}$)	0.7
Initial stack temperature (°C)	60
Initial air stoichiometry	2.9
Initial θ_{45Hz} (°)	30

The experimental results are shown in Figure 4. Comparing the settling times of θ_{45Hz} in Figure 4a,b and Figure 4c,d, the results show that it takes much longer to regulate the water content utilizing the temperature than air stoichiometry. However, the delay of θ_{45Hz} response is within 10 s for both when λ_{O2}* and T* are changed, which has no significant difference. Therefore, the difference in the settling time of two operating conditions causes the difference in settling times of θ_{45Hz}. As shown in Figure 1, the temperature control system utilizes the radiator and the heater to change the coolant temperature. However, the specific heat capacity of the coolant is usually large, leading to hysteresis in temperature regulation. Therefore, the temperature settling time is much longer than that of air stoichiometry for the same regulation requirement of θ_{45Hz}.

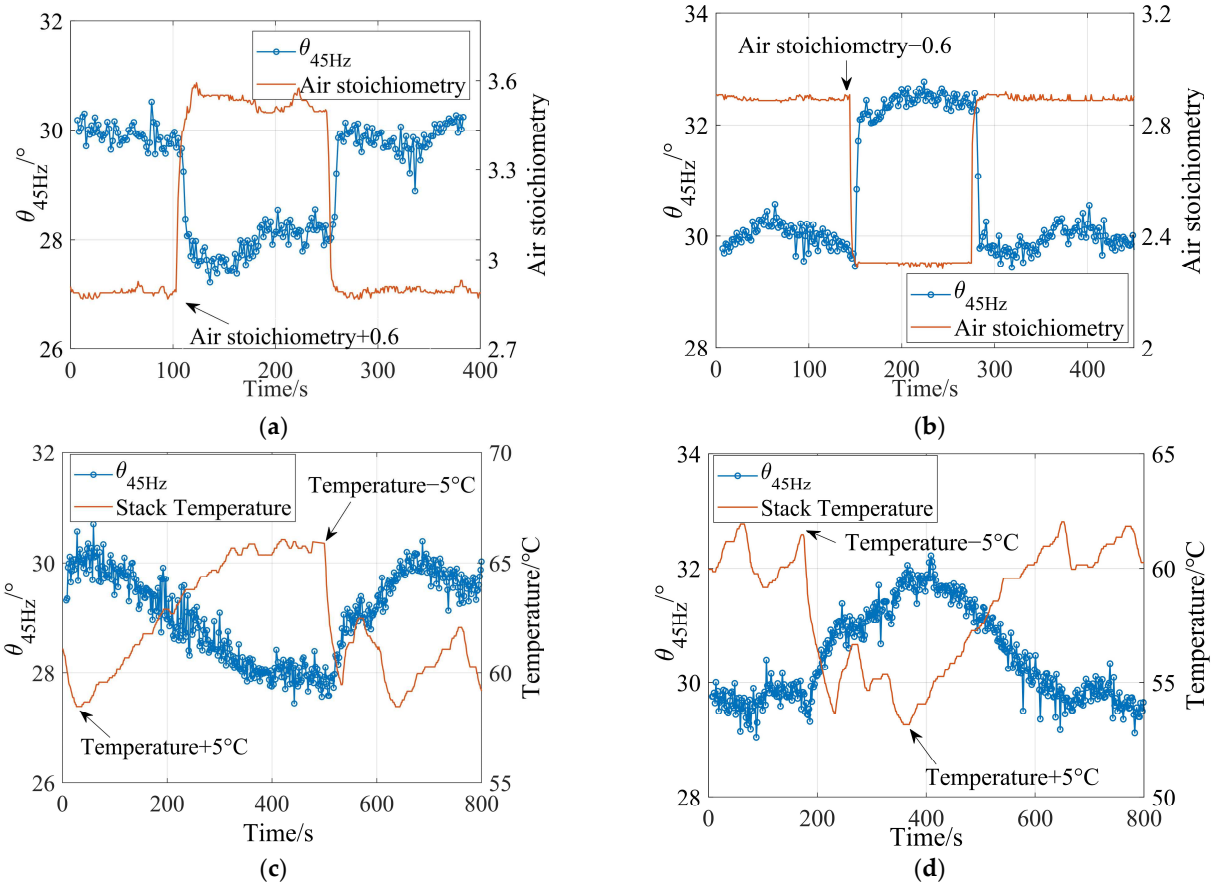

Figure 4. Experimental results of dynamic characteristics of water content. (**a**) Air stoichiometry +0.6; (**b**) air stoichiometry −0.6; (**c**) stack temperature +5 °C; (**d**) stack temperature −5 °C.

In addition, from the influence degree perspective, the difference of θ_{45Hz} between the average value after λ_{O2}* changes and the initial value is about 2.5°, denoted as $\Delta\theta_\lambda$. The difference of θ_{45Hz} between the average value after T* changes and the initial value is about 2°, denoted as $\Delta\theta_T$. Therefore, air stoichiometry is more powerful in regulating the water content than stack temperature within the common operating range. The operating

conditions are dealt with normalization to compare their ability to regulate water content, as expressed by Equation (2).

$$\varphi = \left| \frac{\Delta\theta}{\Delta\gamma/\gamma} \right| \tag{2}$$

where $\Delta\theta$ is the change of $\theta_{45\text{Hz}}$ including $\Delta\theta_\lambda$ and $\Delta\theta_T$. γ is the change of operating conditions. A higher value of φ means that the water content is more sensitive to the corresponding operating condition. φ_λ = 12.08, while φ_T = 24, which means the water content is more sensitive to the change of stack temperature than air stoichiometry.

Based on the research, we fit the transfer functions between the water content and two operating conditions. In order to simplify the fit of the transfer functions, we make the following assumptions: the time required for stack temperature and air stoichiometry regulation can be ignored, which means that both processes are treated as step changes. Based on the dynamic characteristics of $\theta_{45\text{Hz}}$ and assumptions, the transfer functions are fitted according to the first-order inertia element by PID Tuner in MATLAB. The form of the first-order inertia element is:

$$\frac{K}{T_1 s + 1} \tag{3}$$

where K and T_1 are the proportional coefficient and time constant, respectively.

Table 2 lists the fitting results of the transfer functions between the two operating conditions and $\theta_{45\text{Hz}}$ at 0.7 A·cm^{-2}. The negative value of K represents an inverse relationship between $\theta_{45\text{Hz}}$ and both operating conditions: the $\theta_{45\text{Hz}}$ decreases when air stoichiometry and stack temperature increase. In contrast, it increases when air stoichiometry and stack temperature decrease. The fitting results of the two sets of experiments for each of the two operating conditions are similar. Therefore, the fitting results corresponding to the operating conditions can be treated using the numerical averaging method, as shown in Table 3.

Table 2. First-order transfer function fitting results.

Air Stoichiometry	K	T_1	Stack Temperature	K	T_1
+0.6	−3.933	5.154	+5 °C	−0.37	98.7
−0.6	−4.095	5.364	−5 °C	−0.34	88.2

Table 3. First-order transfer function fitting results after numerical averaging.

Parameters	K	T_1
Air stoichiometry	−4.014	5.259
Stack temperature	−0.318	91.73

The dynamic characteristics of the unit step responses of two transfer functions are shown in Table 4. Because the transfer functions are fitted by a first-order inertial element, the overshoot of the unit step responses is zero.

Table 4. Dynamic characteristics of two transfer functions' unit step responses.

Parameters	t_r	$\sigma\%$ [1]
Air stoichiometry	11.57 s	5.259
Stack temperature	201.806 s	91.73

[1] t_r is the rise time. $\sigma\%$ is the overshoot.

3.2.2. Design of the Water Content Regulation Approaches

Figure 5 illustrates the water management system with the detailed water content controller. The output of transfer functions is $\theta_{45\text{Hz}}$, so the impedance-based water content

measurement module is ignored in Figure 5. The water content controller contains three dead zone units and two PI controllers. The design of elements in the water content controller is discussed in order.

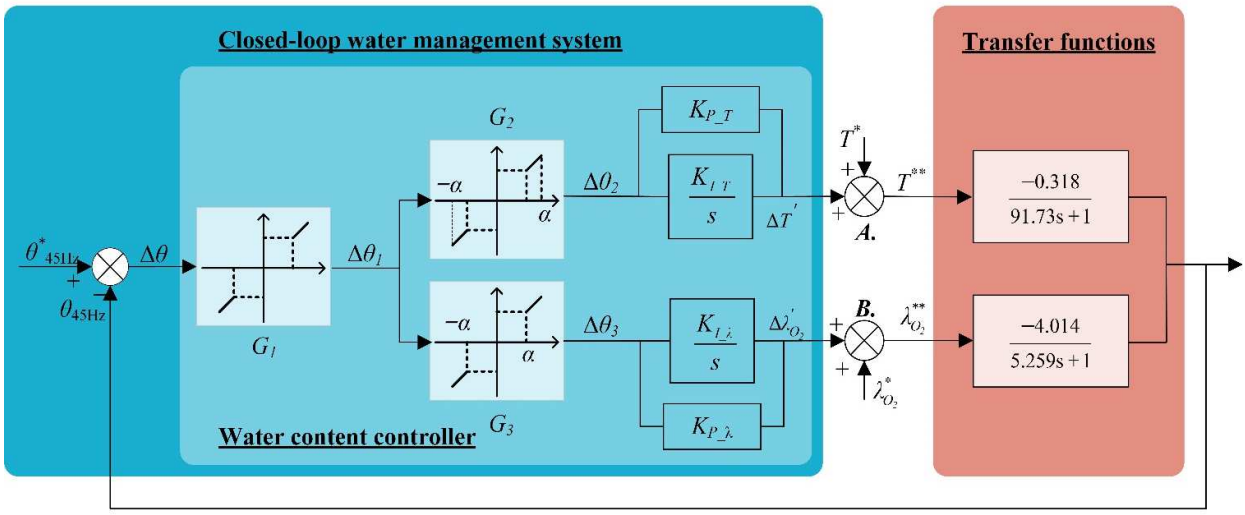

Figure 5. Scheme of the detailed water management system. The blue part is the proposed closed-loop water management system. The orange part is the transfer functions between θ_{45Hz} and the two operating conditions. θ_{45Hz} represents the current water content, and θ^*_{45Hz} is its set value. $\Delta\theta$ is the deviation of θ^*_{45Hz} and θ_{45Hz}. $\Delta\theta_1$, $\Delta\theta_2$, and $\Delta\theta_3$ are the output of the dead zone units G_1, G_2, and G_3, respectively. K_{P_λ} and K_{I_λ} are the proportional and integral coefficients of the PI controller for air stoichiometry, respectively. K_{P_T} and K_{I_T} are the proportional and integral coefficients of the PI controller for the stack temperature, respectively. $\Delta T'$ and $\Delta\lambda_{O2}'$ represent the corrected temperature and air stoichiometry values through PI calculation, respectively. T^* and λ_{O2}^* are the set value of temperature and air stoichiometry, respectively. T^{**} is the output of the comparator at point A. λ_{O2}^{**} is the output of the comparator at point B.

The water content frequently fluctuates in FC systems. Therefore, the regulation target must be extended to a reasonable range around θ^*_{45Hz} to avoid frequent regulation. The range should be narrow enough to ensure that water content must be normal when θ_{45Hz} is within this range. In order to meet the above two requirements simultaneously, we set [30°, 32°] as the target range. Our previous work [32] proved that water content was maintained at normal levels when θ_{45Hz} was in [30°, 32°]. A dead zone unit G_1 is introduced in Figure 5 to generate this interval. The input-output relationship of G_1 is shown in Equation (3).

$$\Delta\theta_1 = \begin{cases} 0, |\Delta\theta| \leq 1^\circ \\ \Delta\theta, |\Delta\theta| > 1^\circ \end{cases} \quad (4)$$

where $\Delta\theta$ is the deviation of the θ_{45Hz} from the θ^*_{45Hz}, and $\Delta\theta_1$ is the output of G_1. $\Delta\theta_1 = 0$ when $|\Delta\theta|$ is less than 1°, which means that the water content does not need to be regulated. In contrast, $\Delta\theta_1 = \Delta\theta$ when $|\Delta\theta|$ is larger than 1°, representing that there is a regulation demand for water content.

$\Delta\theta_1$ is also the input of G_2 and G_3, and it determines which operating conditions are used to regulate the water content. There are many operating conditions that can strongly influence the water content. Air stoichiometry can alter the drainage performance of PEMFC, further significantly affecting liquid water accumulation [24]. Stack temperature determines the saturation vapor pressure inside the stack, significantly affecting water evaporation [18]. The vapor is more likely to be expelled with air or hydrogen than liquid water. Inlet gas humidity affects the water content directly [27]. High pressure of the inlet gas leads to high partial pressure of the water vapor, making the membrane more hydrated [33]. Air stoichiometry and stack temperature are usually adjustable in FC power

systems. Therefore, we adopt air stoichiometry and stack temperature to regulate the water content.

The two operating conditions are applied to meet different regulatory demands. The assignment of regulatory demands considers the differences between the two operating conditions regarding time cost, influence degree to water content, and power loss.

From the time cost perspective, temperature adjustment has a large lag, while air stoichiometry can be regulated quickly. Therefore, air stoichiometry is suitable for conditions where the water content needs to be adjusted quickly and over a wide range. Stack temperature is suitable for a small demand of water content regulation.

From the influence degree to water content, the water content is more sensitive to the change of stack temperature than air stoichiometry. However, the influence degree is not only related to the sensitivity of the water content but also to the regulation time. As shown in Figure 4, adjusting the air metering ratio causes a larger change in $\theta_{45\mathrm{Hz}}$ than the stack temperature during the same time. Air stoichiometry is more suitable for significant regulation because rapidity is also required to avoid serious damage to PEMFC performance. The stack temperature is suitable for low demand because of the water content's sensibility.

From the power loss point of view, adjusting air stoichiometry in power systems often depends on the air compressor's speed change. However, the air compressor is a high-power auxiliary component whose power is about 3–14 kW. Frequent changes in compressor speed result in additional power loss to FC systems. In power systems, the cooling fans that adjust temperature are rated at approximately 500 W. By comparison, the power loss caused by adjusting the cooling fans' speed is much smaller than that caused by the air compressor adjustment.

Therefore, the assignment of regulatory demands is as follows:

- Air stoichiometry is applied to meet conditions where the water content needs to be significantly regulated.
- Stack temperature is used to meet the low demanding case of water content regulation.

Dead zone units G_2 and G_3 are employed to achieve cooperation between the two operating conditions. Only air stoichiometry or stack temperature is adopted to regulate the water content during a control cycle. The input-output relationships of G_2 and G_3 are shown in Equations (4) and (5).

$$\Delta\theta_2 = \begin{cases} 0, \ |\Delta\theta_1| \leq 1^\circ \\ \Delta\theta_1, \ 1^\circ < |\Delta\theta_1| \leq \alpha^\circ \\ 0, \ |\Delta\theta_1| > \alpha^\circ \end{cases} \tag{5}$$

$$\Delta\theta_3 = \begin{cases} 0, \ |\Delta\theta_1| \leq \alpha^\circ \\ \Delta\theta_1, \ |\Delta\theta_1| > \alpha^\circ \end{cases} \tag{6}$$

where $\Delta\theta_1$, $\Delta\theta_2$, and $\Delta\theta_3$ are the output of G_1, G_2, and G_3, respectively. α is the boundary value between G_2 and G_3. $\Delta\theta_2$ equals $\Delta\theta_1$ when $|\Delta\theta_1|$ is in the interval of $(1, \alpha]$. In contrast, $\Delta\theta_2$ equals zero when $|\Delta\theta_1|$ is in any other interval, which means no regulation of stack temperature is performed. $\Delta\theta_3$ is equal to $\Delta\theta_1$ when $|\Delta\theta_1|$ is larger than α. In contrast, $\Delta\theta_3$ is equal to zero when $|\Delta\theta_1|$ is in any other interval, which means no regulation of air stoichiometry is performed. Moreover, the determination of α is based on the ability of two operating conditions to regulate the water content.

From the Cannikin Law, the setting of α refers to the smaller of $\Delta\theta_T$ or $\Delta\theta_\lambda$. Compared $\Delta\theta_T$ with $\Delta\theta_\lambda$, it can be seen that the ability of stack temperature to regulate water content is more limited than air stoichiometry in setting operating range. In addition, when $\theta_{45\mathrm{Hz}}$ is in $[\theta^*_{45\mathrm{Hz}}-1^\circ, \theta^*_{45\mathrm{Hz}}+1^\circ]$, there is no regulatory requirement for water content. Therefore, α is set to 3°, equal to $\Delta\theta_T+1^\circ$, which means:

- The water management system regulates the water content by changing stack temperature when $|\Delta\theta_1|$ is larger than 1° but smaller than 3°.

- The water management system regulates the water content by changing air stoichiometry when $|\Delta\theta_1|$ is larger than 3°.

The output of G_2 and G_3 are the input of temperature and air stoichiometry PI controllers, respectively. The form of the PI control algorithm applied in the water content controller is shown in Figure 5. Parameters of the PI algorithm are often determined by the engineering rectification approach. However, the theoretical calculation approach can provide a better theoretical basis for determining PI parameters. The theoretical calculation approach is based on the transfer functions between the water content and two operating conditions. According to the obtained transfer functions shown in Table 4, the optimal PI parameters for two operating conditions are calculated with the help of Control System Tuner in MATLAB: $K_{P\_\lambda} = -0.625$, $K_{I\_\lambda} = -0.116$, $K_{P\_T} = -4.403$, and $K_{I\_T} = -0.07$. However, the above PI parameters are only theoretical values obtained from simplified transfer functions. According to the results of the theoretical calculation approach, the final PI parameters are set as $K_{P\_\lambda} = -1$, $K_{I\_\lambda} = -0.1$, $K_{P\_T} = -2.5$, and $K_{I\_T} = -0.02$ through the engineering rectification approach.

4. Experimental Validation of the Control Strategy

In order to verify the effectiveness of the proposed closed-loop water management system, this section conducts constant-load experiments with disturbance and variable-load experiments. Changes in FC systems operating conditions and load current can easily cause large fluctuations in water content, where the proposed water management approach should effectively keep the water content within the target range.

4.1. Results of Constant-Load Experiments

In this section, we simulate the situations where the operating conditions are perturbed by artificially changing λ_{O2}* and T* mentioned in Figure 1. All experiments are conducted in the constant current density 0.7 A·cm^{-2}. All experiments' initial operating conditions are constant to guarantee the same initial θ_{45Hz}. A control cycle is fifteen seconds. The specific changes in the operating conditions are a 5 °C increase in stack temperature, a 5 °C decrease in stack temperature, a 0.4 increase in air stoichiometry, and a 0.4 decrease in air stoichiometry. Practically, only one operation condition is perturbed for each experiment. The initial experimental parameters are shown in Table 5.

Table 5. Setting of the standard experimental parameters.

Parameters	Value
Current density (A·cm^{-2})	0.7
Initial stack temperature (°C)	60
Initial air stoichiometry	2.8
Initial θ_{45Hz} (°)	30
Control cycle (s)	15

Figure 6 shows the change of parameters, including average cell voltage, θ_{45Hz}, air stoichiometry, and stack temperature. The experiment in Figure 6a simulates the case of increasing stack temperature. T* is adjusted to 65 °C (at the 30th second) after PEMFC has operated in normal state. At the same time, the water management system starts running. During the 1st to 28th control cycles, θ_{45Hz} gradually decreases as the temperature increases, while the average cell voltage gradually increases. In the 29th control cycle, θ_{45Hz} is lower than the normal state and in the temperature regulation range [28°, 30°]. In the 29th to 35th control cycle, stack temperature is regulated according to $\Delta\theta$. During the regulation process, stack temperature is gradually reduced, so the saturated vapor pressure decreases, the internal liquid water increases, and θ_{45Hz} rises. After the 35th control cycle, θ_{45Hz} is regulated back to the target range, indicating that the water management system has regulated the water content back to the normal state. Meanwhile, stack temperature is reduced to the initial value, and the average cell voltage returns to the initial value.

Similarly, Figure 6b shows the experimental results of lowering stack temperature, which is the opposite regulation process of Figure 6a.

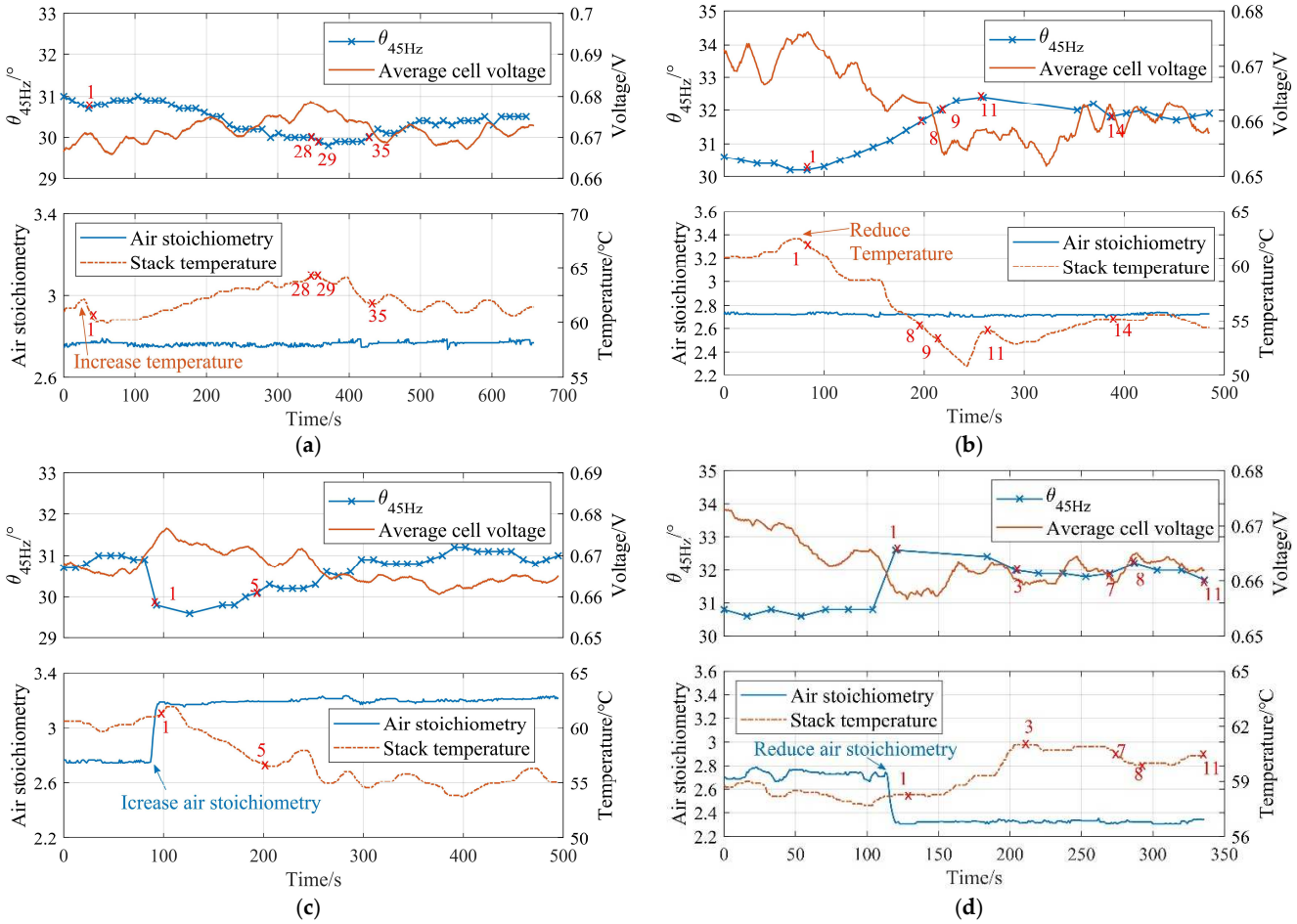

Figure 6. Constant-load experimental results. (**a**) Increased stack temperature; (**b**) decreased stack temperature; (**c**) increased air stoichiometry; (**d**) decreased air stoichiometry. The red numbers represent the typical control cycles.

The experiment in Figure 6c simulates the case of increasing air stoichiometry. Air stoichiometry is increased by 0.4 at the 90th second after PEMFC has operated in normal state. At the same time, the water management system starts running. In the first control cycle, θ_{45Hz} drops rapidly below 30°, and the average cell voltage of the PEMFC rises significantly. The rise in air stoichiometry promotes the drainage process of PEMFC, which causes more water to be carried out. According to $\Delta\theta$, which is less than 3° in the first control cycle, stack temperature is adopted to regulate water content. In the 1st to 5th control cycles, the FC test system keeps reducing stack temperature under the calculation of the PI controller. The reduction of stack temperature leads to the vapor's condensation, increasing water content. Furthermore, the average cell voltage gradually decreases. After the 5th control cycle, θ_{45Hz} is regulated back to the normal interval and is similar to the initial phase angle. However, it is easy to observe that θ_{45Hz} is still changing due to the hysteresis and fluctuation of the stack temperature. Finally, θ_{45Hz} is steady near 31° in the 15th control cycle, while the average cell voltage is constant near 0.665 V. Therefore, it can be considered that the water management system has achieved the regulation target in the 5th control cycle. Similarly, Figure 6d shows the results for the decrease in air stoichiometry, which is the opposite regulation process of Figure 6c.

The key parameters of the above experiments are statistically presented in Table 6 for cross-sectional comparison. The $|\Delta\theta|_{max}$ is less than 3° in all four experiments, so the

constant-load experiments only trigger the temperature adjustment in the water management system. As a result, all experiments only use no more than six cycles to regulate $\theta_{45\mathrm{Hz}}$ to [30°, 32°]. Therefore, it can be considered that (1) changing the stack temperature can meet the small demand of the water content regulation; (2) when the operating conditions change, the water management system can effectively solve the disturbance of the water content and regulate it to the target range.

Table 6. Statistics of constant-load experiments.

Perturbed Parameters	Increased Temperature	Reduced Temperature	Increased Air Stoichiometry	Reduced Air Stoichiometry
θ_{abn}	29.8°	32.4°	29.6°	32.6°
$\lvert\Delta\theta\rvert_{\max}$	1.2°	1.4°	1.4°	1.6°
C_{total} [1]	6	5	4	6

[1] θ_{abn} represents the value of $\theta_{45\mathrm{Hz}}$ farthest from $\theta^*_{45\mathrm{Hz}}$. $\lvert\Delta\theta\rvert_{\max}$ is the maximum error of $\theta_{45\mathrm{Hz}}$ compared to $\theta^*_{45\mathrm{Hz}}$. C_{total} represents the total control periods for $\theta_{45\mathrm{Hz}}$ regulated to the target range.

4.2. Results of Variable-Load Experiments

This section simulates the limit of the variable-load process, i.e., the operating conditions are controlled by the water management system instead of following the load variation. According to the load current variation, experiments can be divided into two categories: loading and down-loading. The current density is reduced from 0.7 A·cm^{-2} to 0.4 A·cm^{-2} in the down-loading experiment. In the loading experiment, it is increased from 0.7 A·cm^{-2} to 0.8 A·cm^{-2}. The initial current density and stack temperature are the same as constant-load experiments, as shown in Table 5. In variable-load experiments, the initial air stoichiometry and $\theta_{45\mathrm{Hz}}$ differ from the constant-load experiments. The initial air stoichiometry is 2.7 and the initial $\theta_{45\mathrm{Hz}}$ is 31°.

Figure 7 illustrates the change in average cell voltage, $\theta_{45\mathrm{Hz}}$, air stoichiometry, and stack temperature. Figure 7a shows the regulation process under the down-loading condition. The current density is reduced to 0.4 A·cm^{-2} at the 70th second. At the same time, the water management system starts running. In the 2nd control cycle, $\theta_{45\mathrm{Hz}}$ is less than 30°, while the average cell voltage increases rapidly from 0.66 V to 0.74 V. The reduction in the current density makes the water-producing capability of PEMFC decrease. Meanwhile, the operating conditions are still at high levels for 0.7 A·cm^{-2}. According to Equation (1), although the air mass flow is constant, air stoichiometry rises because of the reduction of load current. Therefore, the water inside the PEMFC is excessively drained. In addition, $\lvert\Delta\theta\rvert$ is larger than 3° during the 2nd cycle, representing that the current state is in the range of air stoichiometry regulation ($\theta_{45\mathrm{Hz}} < 28°$). According to the results of the PI calculation, the water management system reduces air stoichiometry. Then, the $\theta_{45\mathrm{Hz}}$ recovers to 28.7°, and $\lvert\Delta\theta\rvert$ is measured as less than 3° during the 3rd control cycle, representing that the current state is in the temperature regulation range [28°, 30°]. $\Theta_{45\mathrm{Hz}}$ rises during the 4th to 17th control cycles because of the decrease in stack temperature. After the 17th control cycle, the average cell voltage returns to a steady state, while $\theta_{45\mathrm{Hz}}$ is not always in the normal range because of fluctuations in temperature. The water management system tunes the stack temperature slightly according to $\Delta\theta$. The final $\theta_{45\mathrm{Hz}}$ keeps fluctuating in the range of 29.8° to 30.1°. However, water content is still in the normal state when $\theta_{45\mathrm{Hz}}$ is 29.8°. Therefore, it can be concluded that the water content is regulated to the normal state after the 17th control cycle.

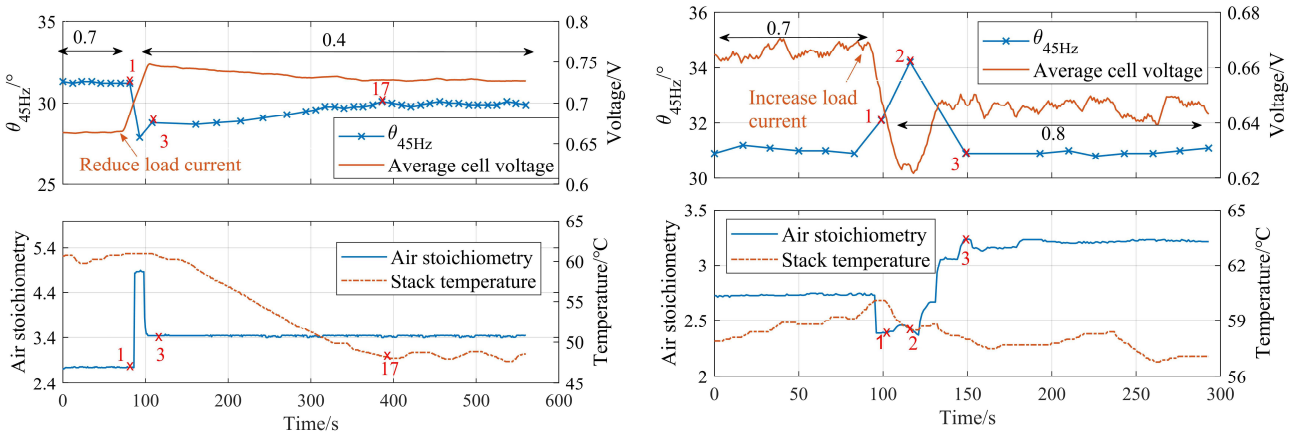

(**a**) (**b**)

Figure 7. Variable-load experimental results. (**a**) Down-loading experiment; (**b**) loading experiment. The red numbers represent the typical control cycles. The black numbers represent the current densities of the stack.

Figure 7b shows the results of the loading condition. The current density is increased to 0.8 A·cm^{-2} at the 90th second. At the same time, the water management system starts running. In the 1st control cycle, θ_{45Hz} is above 32°. The water-producing capability of PEMFC rises after loading. Meanwhile, the operating conditions remain at low levels of 0.7 A·cm^{-2}. Air stoichiometry decreases rapidly because of the rise of load current. Therefore, PEMFC is over-humidified with a large accumulation of liquid water. In addition, the average cell voltage drops rapidly from 0.66 V to 0.625 V. During the 1st control cycle, $|\Delta\theta|$ appears to be less than 3°, representing the current state is in the temperature regulation range [32°, 34°]. According to the results of the PI calculation, the water management system orders to raise the stack temperature by 0.4 °C. However, because of the hysteresis, the stack temperature decreases instead, resulting in a continued increase in water content. In the 2nd control cycle, $|\Delta\theta|$ is higher than 3°, which means that the current state enters the interval of air stoichiometry regulation (θ_{45Hz} > 34°). The water management system commands an increase in air stoichiometry to make the excess water be removed quickly. Therefore, the water content decreases rapidly. After the 3rd control cycle, θ_{45Hz} returns to the target interval, and the average cell voltage returns to constant.

Table 7 provides the key statistics to compare the two sets of experiments horizontally. The $|\Delta\theta|_{max}$ is larger than 3° in both variable-load experiments, indicating that both experiments trigger the adjustment of air stoichiometry in the water management system. Unlike constant-load experiments, the water content is regulated by the cooperation of two operating conditions in variable-load experiments. Limited by the temperature adjustment devices, the down-loading experiment takes fifteen cycles to regulate the water content. In contrast, the loading experiment takes only two cycles. Two operating conditions successfully regulate the water content according to the control strategy. The proposed water management system effectively solves the significant disturbance of the water content in variable-load experiments.

Table 7. Variable-load experiment statistics.

Perturbed Parameters	Down-Loading	Loading
θ_{abn}	27.9	34.2
$\|\Delta\theta\|_{max}$	3.1	3.2
C_{total}	15	2

4.3. Discussion

The purpose of validation experiments is to verify the effectiveness of the proposed water management system. From the perspective of the complexity of water management, the variable-load and constant-load experiments are different. The water content is determined by the stack's water production capacity, drainage capacity and external humidification. The current density determines the water production capacity of the stack. Compared to the variable-load experiment, the constant-load experiment only affects the drainage and external humidification by adjusting the operating conditions but does not change the water production capacity. Therefore, with the same water production capacity of the stack, only the drainage and external humidification need to be balanced to complete the water content regulation. However, in the variable load experiment, the balance between the three is seriously damaged, and the water management is more complicated because of the change in water production capacity. This hypothesis can be verified by comparing the control cycles of the constant-load and variable-load experiments.

However, it is interesting that the control periods used for the regulation process of loading and down-loading experiments seem to be two opposite extremes. Although the water content is eventually regulated to the target interval in all experiments, the water management system takes eighteen control cycles in the down-loading experiment, while it takes only two in the loading experiment.

Like the loading experiment, only one cycle is used to adjust the air stoichiometry for the down-loading experiment. However, in the down-loading experiment, the air stoichiometry is adjusted more than in the loading experiment, while the water content response is smaller. This phenomenon is related to the stack's water production and drainage capacity. In the loading experiment, the water production capacity of the stack is increased, and the water content needs to be reduced. Increasing the air stoichiometry can significantly raise the drainage capacity to balance the water production capacity. In the down-loading experiment, the water production capacity decreases as the current density reduces, and the water content needs to be increased. Although the air stoichiometry is reduced in time, it can only reduce drainage. The humidification of the stack remains low. Therefore, in the down-loading experiment, the change of water content due to the regulation of the air stoichiometry is smaller than in the loading experiment. However, the proposed water management system has considered this issue. This system lowers the temperature to increase the condensation of liquid water and reduce the back-diffusion process of water in the membrane, which helps the humidification of the stack. However, limited by the equipment, the slow regulation of temperature causes excessive time costs in the down-loading experiment.

The results of variable-load experiments verify that in such complex regulation cases, the closed-loop water management system still effectively keeps the water content within the target range. Therefore, the closed-loop water management system is effective in controlling the water content. The performance and durability of PEMFC are promoted by the long-term operation of the stack with normal water content. Limited by the experimental equipment and conditions, this research did not explore the specific extent of the proposed system's contribution to the durability of PEMFC. In the future, we will further investigate the effect of the water management system on the durability of PEMFC.

Although the proposed water management system has proven effective, its applicability should be considered in FC power systems. This system mainly contains the measurement method based on the phase of the single-frequency impedance and the PI controllers of the air stoichiometry and temperature. The measurement method based on the phase of the single-frequency impedance is suitable for FC power systems because it is simple and can correspond numerically well to the water content. The air stoichiometry and temperature are generally adjustable in FC power systems. Meanwhile, the PI algorithm has been widely used in the industry. Therefore, the proposed water management system is suitable for applying to the FC power systems in the transportation field.

5. Conclusions and Prospects

The purpose of this paper was to control the water content of the FC system within a reasonable range. For the above purpose, a closed-loop water management system was proposed based on the phase angle of single-frequency impedance. Results of research on the open-loop characteristics of water content indicated that water content was more sensitive to the change in temperature than the change in air stoichiometry. Moreover, the air stoichiometry was suitable for large regulation requirements of water content because adjusting air stoichiometry was quicker than stack temperature. The stack temperature was suitable to involve the small regulation demands. In the validation experiments, the water management of variable-load experiments was more complicated than constant-load experiments due to the damage to the balance of the stack's water production capacity, drainage capacity and external humidification. In these complex cases, the water content regulation results indicated that the closed-loop water management system could control the water content to the target range within a 3% deviation from the desired value. This study provides a basis for further optimization of PEMFC water management.

In the future, we will further investigate the effect of the water management system on the durability of PEMFC. The parameters related to durability should be considered. Some comparative experiments will be applied to this research.

Author Contributions: Conceptualization, K.L., X.X., and Z.L.; methodology, X.X., K.L., and Z.L.; software, X.X. and Z.L.; validation, X.X., Z.L., and J.C.; formal analysis, X.X., K.L., and Z.L.; investigation, X.X., Z.L., R.W., and K.L.; resources, K.L.; data curation, X.X., Z.L., J.C., and R.W.; writing—original draft preparation, X.X. and Z.L.; writing—review and editing, X.X. and K.L.; visualization, X.X. and K.L.; supervision, K.L., J.C., and R.W.; project administration, K.L., J.C., and R.W.; funding acquisition, K.L. All authors have read and agreed to the published version of the manuscript.

Funding: This research was funded by the National Key Research and Development Program of China, grant number 2021YFB2500500.

Data Availability Statement: Data used in the current work are from the literature and all sources can be found in the references list.

Acknowledgments: The authors would like to thank the editor and the anonymous reviewers who gave constructive comments and helped to improve the quality of this article. The same appreciation goes to the Hydrogen and fuel cell institute and Yaqi Han who provided some writing advice.

Conflicts of Interest: The authors declare no conflict of interest. The funders had no role in the design of the study; in the collection, analyses, or interpretation of data; in the writing of the manuscript, or in the decision to publish the results.

References

1. Yin, C.; Cao, J.; Tang, Q.; Su, Y.; Wang, R.; Li, K.; Tang, H. Study of internal performance of commercial-size fuel cell stack with 3D multi-physical model and high resolution current mapping. *Appl. Energy* **2022**, *323*, 119567. [CrossRef]
2. Barnoon, P.; Toghraie, D.; Mehmandoust, B.; Fazilati, M.A.; Eftekhari, S.A. Natural-forced cooling and Monte-Carlo multi-objective optimization of mechanical and thermal characteristics of a bipolar plate for use in a proton exchange membrane fuel cell. *Energy Rep.* **2022**, *8*, 2747–2761. [CrossRef]
3. Su, Y.; Yin, C.; Hua, S.; Wang, R.; Tang, H. Study of cell voltage uniformity of proton exchange membrane fuel cell stack with an optimized artificial neural network model. *Int. J. Hydrogen Energy* **2022**, *47*, 29037–29052. [CrossRef]
4. Schmittinger, W.; Vahidi, A. A review of the main parameters influencing long-term performance and durability of PEM fuel cells. *J. Power Sources* **2008**, *180*, 1–14. [CrossRef]
5. Lebreton, C.; Benne, M.; Damour, C.; Yousfi-Steiner, N.; Grondin-Perez, B.; Hissel, D.; Chabriat, J.P. Fault Tolerant Control Strategy applied to PEMFC water management. *Int. J. Hydrogen Energy* **2015**, *40*, 10636–10646. [CrossRef]
6. Ous, T.; Arcoumanis, C. Degradation aspects of water formation and transport in Proton Exchange Membrane Fuel Cell: A review. *J. Power Sources* **2013**, *240*, 558–582. [CrossRef]
7. Ijaodola, O.S.; El-Hassan, Z.; Ogungbemi, E.; Khatib, F.N.; Wilberforce, T.; Thompson, J.; Olabi, A.G. Energy efficiency improvements by investigating the water flooding management on proton exchange membrane fuel cell (PEMFC). *Energy* **2019**, *179*, 246–267. [CrossRef]
8. Moçotéguy, P.; Ludwig, B.; Beretta, D.; Pedersen, T. Study of the impact of water management on the performance of PEMFC commercial stacks by impedance spectroscopy. *Int. J. Hydrogen Energy* **2020**, *45*, 16724–16737. [CrossRef]

9. Peng, Y.; Mahyari, H.M.; Moshfegh, A.; Javadzadegan, A.; Toghraie, D.; Shams, M.; Rostami, S. A transient heat and mass transfer CFD simulation for proton exchange membrane fuel cells (PEMFC) with a dead-ended anode channel. *Int. Commun. Heat Mass Transf.* **2020**, *115*, 104638. [CrossRef]
10. Pei, P.; Chen, H. Main factors affecting the lifetime of Proton Exchange Membrane fuel cells in vehicle applications: A review. *Appl. Energy* **2014**, *125*, 60–75. [CrossRef]
11. Yan, C.; Chen, J.; Liu, H.; Kumar, L.; Lu, H. Health Management for PEM Fuel Cells Based on an Active Fault Tolerant Control Strategy. *IEEE Trans. Sustain. Energy* **2020**, *12*, 1311–1320. [CrossRef]
12. Debenjak, A.; Gašperin, M.; Pregelj, B.; Atanasijević-Kunc, M.; Petrovčič, J.; Jovan, V. Detection of Flooding and Drying inside a PEM Fuel Cell Stack. *Stroj. Vest.* **2013**, *59*, 56–64. [CrossRef]
13. Yuan, X.Z.; Song, C.; Wang, H.; Zhang, J. *Electrochemical Impedance Spectroscopy in PEM Fuel Cells: Fundamentals and Applications*; Springer: London, UK, 2010; pp. 193–258.
14. Fouquet, N.; Doulet, C.; Nouillant, C.; Dauphin-Tanguy, G.; Ould-Bouamama, B. Model based PEM fuel cell state-of-health monitoring via ac impedance measurements. *J. Power Sources* **2006**, *159*, 905–913. [CrossRef]
15. Gebregergis, A.; Pillay, P.; Rengaswamy, R. PEMFC fault diagnosis, modeling, and mitigation. *IEEE Trans. Ind. Appl.* **2010**, *46*, 295–303. [CrossRef]
16. Song, M.; Pei, P.; Zha, H.; Xu, H. Water management of proton exchange membrane fuel cell based on control of hydrogen pressure drop. *J. Power Sources* **2014**, *267*, 655–663. [CrossRef]
17. Ous, T.; Arcoumanis, C. Visualisation of water accumulation in the flow channels of PEMFC under various operating conditions. *J. Power Sources* **2009**, *187*, 182–189. [CrossRef]
18. Cadet, C.; Jemei, S.; Druart, F.; Hissel, D. Diagnostic tools for PEMFCs: From conception to implementation. *Int. J. Hydrogen Energy* **2014**, *39*, 10613–10626. [CrossRef]
19. Kurz, T.; Hakenjos, A.; Krämer, J.; Zedda, M.; Agert, C. An impedance-based predictive control strategy for the state-of-health of PEM fuel cell stacks. *J. Power Sources* **2008**, *180*, 742–747. [CrossRef]
20. Kitamura, N.; Manabe, K.; Nonobe, Y.; Kizaki, M. *Development of Water Content Control System for Fuel Cell Hybrid Vehicles Based on AC Impedance*; SAE Technical Paper; 2010-01-1088; SAE: New York, USA, 2010.
21. Hong, P. *Water Content Estimation and Control of PEM Fuel Cell Stack and the Individual Cell in Vehicle*; Springer Nature: Berlin/Heidelberg, Germany, 2022; pp. 12–40.
22. Le Canut, J.M.; Abouatallah, R.M.; Harrington, D.A. Detection of membrane drying, fuel cell flooding, and anode catalyst poisoning on PEMFC stacks by electrochemical impedance spectroscopy. *J. Electrochem. Soc.* **2006**, *153*, A857. [CrossRef]
23. Zhang, L.; Pan, M.; Quan, S. Model predictive control of water management in PEMFC. *J. Power Sources* **2008**, *180*, 322–329. [CrossRef]
24. Chen, X.; Xu, J.; Liu, Q.; Chen, Y.; Wang, X.; Li, W.; Ding, Y.; Wan, Z. Active disturbance rejection control strategy applied to cathode humidity control in PEMFC system. *Energy Convers. Manag.* **2020**, *224*, 113389. [CrossRef]
25. Hosseini, M.; Afrouzi, H.H.; Arasteh, H.; Toghraie, D. Energy analysis of a proton exchange membrane fuel cell (PEMFC) with an open-ended anode using agglomerate model: A CFD study. *Energy* **2019**, *188*, 116090. [CrossRef]
26. Santarelli, M.G.; Torchio, M.F.; Calı, M.; Giaretto, V. Experimental analysis of cathode flow stoichiometry on the electrical performance of a PEMFC stack. *Int. J. Hydrogen Energy* **2007**, *32*, 710–716. [CrossRef]
27. Amirinejad, M.; Rowshanzamir, S.; Eikani, M.H. Effects of operating parameters on performance of a proton exchange membrane fuel cell. *J. Power Sources* **2006**, *161*, 872–875. [CrossRef]
28. Yuan, H.; Dai, H.; Ming, P.; Wang, X.; Wei, X. Quantitative analysis of internal polarization dynamics for polymer electrolyte membrane fuel cell by distribution of relaxation times of impedance. *Appl. Energy* **2021**, *303*, 117640. [CrossRef]
29. Lu, H.; Chen, J.; Yan, C.; Liu, H. On-line fault diagnosis for proton exchange membrane fuel cells based on a fast electrochemical impedance spectroscopy measurement. *J. Power Sources* **2019**, *430*, 233–243. [CrossRef]
30. Mei, B.; Barnoon, P.; Toghraie, D.; Su, C.H.; Nguyen, H.C.; Khan, A. Energy, exergy, environmental and economic analyzes (4E) and multi-objective optimization of a PEM fuel cell equipped with coolant channels. *Renew. Sustain. Energy Rev.* **2022**, *157*, 112021. [CrossRef]
31. Pukrushpan, J.T.; Stefanopoulou, A.G.; Peng, H. *Control of Fuel Cell Power Systems: Principles, Modeling, Analysis and Feedback Design*; Springer Science & Business Media: Berlin/Heidelberg, Germany, 2004; pp. 31–36.
32. Liao, Z. Research on Closed-Loop Water Management Technology of Proton Exchange Membrane Fuel Cell based on AC Impedance. Master's Thesis, University of Electronic Science and Technology of China, Chengdu, China, 2022.
33. Bao, C.; Ouyang, M.; Yi, B. Analysis of water management in proton exchange membrane fuel cells. *Tsinghua Sci. Technol.* **2006**, *11*, 54–64. [CrossRef]